The crystal structure of a cross-linked actin dimer suggests a detailed molecular interface in F-actin

Dmitry S. Kudryashov*†, Michael R. Sawaya*†, Helty Adisetiyo*, Todd Norcross*, György Hegyi‡, Emil Reisler*, and Todd O. Yeates*§

*Department of Chemistry and Biochemistry and Molecular Biology Institute, University of California, Los Angeles, CA 90095; and ‡Department of Biochemistry, Eötvös Lorand University, H-1088, Budapest, Hungary

Communicated by David S. Eisenberg, University of California, Los Angeles, CA, July 30, 2005 (received for review July 7, 2005)

The 2.5-Å resolution crystal structure is reported for an actin dimer, composed of two protomers cross-linked along the longitudinal (or vertical) direction of the F-actin filament. The crystal structure provides an atomic resolution view of a molecular interface between actin protomers, which we argue represents a near-native interaction in the F-actin filament. The interaction involves subdomains 3 and 4 from distinct protomers. The atomic positions in the interface visualized differ by 5–10 Å from those suggested by previous models of F-actin. Such differences fall within the range of uncertainties allowed by the fiber diffraction and electron microscopy methods on which previous models have been based. In the crystal, the translational arrangement of protomers lacks the slow twist found in native filaments. A plausible model of F-actin can be constructed by reintroducing the known filament twist, without disturbing significantly the interface observed in the actin dimer crystal.

actin crystal structure | F-actin filament | motor proteins

Actin is one of the most highly conserved proteins in nature, where it plays key roles in contraction, cell shape and motility, and subcellular organization. Actin's myriad functions are regulated by protein-protein interactions. Besides interacting with an enormously diverse set of other cellular proteins (1), actin's most critical functions arise from its interactions with itself as it assembles to form F-actin filaments. Because actin carries out its cellular functions through its filamentous form, knowing the detailed structure of actin filaments is an important step in achieving a mechanistic understanding of actin function.

Our understanding of actin has been advanced greatly by intensive investigation into its three-dimensional (3D) structure. Because the filamentous form of actin is essentially incompatible with the growth of 3D crystals, crystallographic studies have focused on actin in its monomeric form. The 3D structure of monomeric actin (G-actin) was determined first by Kabsch *et al.* (2) as a complex, with DNase I serving as a polymerization inhibitor. The crystal structure of monomeric actin has since been determined at atomic resolution under a variety of conditions, varying, for example, in actin isoform (3), the identity of the bound nucleotide (4, 5), and in the identity of the other proteins (6, 7) or small molecules added as polymerization inhibitors (8, 9). As a consequence, the structure of the actin monomer (G-actin) is understood in considerable detail, although some important issues remain open regarding nucleotide-dependent changes in G-actin structure, including a possible transition between the open and closed nucleotide cleft conformations and the order–disorder shift of the DNase I-binding loop (4, 7, 10).

Structural models of the actin filament have derived mainly from methods other than crystallography. The first structural model of F-actin was obtained by Holmes *et al.* (11), by using fiber-diffraction data extending to 8.4-Å resolution to determine the approximate orientations and positions of actin protomers in the filament. The F-actin filament has been analyzed in numerous subsequent imaging studies, by electron microscopy (EM) with negative staining and cryoelectron microscopy (12–17). These imaging studies have supported the basic features of the Holmes model and have led to structural refinements and variations under differing circumstances and conditions.

The basic elements of the Holmes model for F-actin, and similar models based on subsequent imaging experiments, have been supported by biophysical experiments and by data on evolutionarily related proteins. Numerous cross-linking experiments provide supporting evidence for residues expected to be proximal based on models of F-actin. Cross-linking data are available both for protomers related in the lateral direction [i.e., sideways between the two helical strands (18–20)] and for protomers related in the longitudinal direction [i.e., along one vertical strand of the two stranded F-actin helix (19, 21)]. Data from synchrotron x-ray radiolysis experiments, probing the reactivity of solvent-accessible residues, are also consistent with structural models (22). Finally, recent crystal structures of bacterial proteins involved in cell-shape determination (MreB) and cell division (ParM) have revealed the evolutionary relationships of these prokaryotic proteins to actin (23, 24). These prokaryotic proteins form linear (23) or helical (24) filaments with their protomers in an arrangement similar to that seen in F-actin strands according to structural models.

Despite a general consensus regarding the validity of current models for F-actin, the problem of atomic-level detail remains. Although the atomic resolution structure of the actin protomer by itself is known, a detailed understanding of how these protomers contact each other in the filament is limited by the precision with which the orientations and positions of the protomers can be determined from fiber diffraction and EM data, extending from 8- to 10-Å resolution in the best cases (11, 25). The information on interprotomer contacts is important in particular for understanding the binding of many proteins to actin and how these binding events are facilitated through alternate arrangements of these contacts.

The need for high-resolution data relating to F-actin has promoted efforts to determine crystal structures of multiple actin protomers in an F-actin-like arrangement. Dawson *et al.* (26) were successful in crystallizing three actin protomers cross-linked together. However, the crystal structure revealed that protomer rearrangements had led to a dissociation of the interfaces expected in the F-actin filament. Klenchin *et al.* (27) described the structure of an actin dimer coordinated by the marine macrolide toxin, swinholide A; however, the twofold symmetry of the complex is very different from the screw symmetry of native actin fibers. Bubb *et al.* (28) determined the

Freely available online through the PNAS open access option.

Abbreviation: ANP, *N*-(4-azido-2-nitrophenyl) putrescine.

Data deposition: The atomic coordinates have been deposited in the Protein Data Bank, www.pdb.org (PDB ID code 2A5X).

†D.S.K. and M.R.S. contributed equally to this work.

§To whom correspondence should be addressed. E-mail: yeates@mbi.ucla.edu.

crystal structure of an actin dimer in which the protomers are held together in an antiparallel arrangement. Although the significance of this antiparallel actin dimer remains an open question, its structure does not relate to the native F-actin interfaces, in which protomers are arranged head-to-tail in parallel filaments. Finally, a recent structure of the protein formin in complex with two actin protomers has been used to provide some detail about the lateral or side-by-side interaction between two actin protomers in adjacent strands of the F-actin filament (29). Here, we report a crystal structure of a longitudinal actin dimer, which illuminates how actin protomers most likely touch each other along the vertical direction within the individual strands of the F-actin filament. Resulting structural models for F-actin are discussed.

Materials and Methods

Skeletal Actin. Actin from rabbit back muscle was prepared according to Spudich and Watt (30) (see *Supporting Materials and Methods*, which is published as supporting information on the PNAS web site).

Generation of Yeast Actin Mutants T203C/C374S and D288C. Point mutations were introduced into the sequence of yeast actin by using the QuikChange Site-Directed Mutagenesis kit (Stratagene). Mutants were purified and cross-linked as described in *Supporting Materials and Methods*.

Preparation of Actin Dimers. The longitudinal dimer of rabbit skeletal actin was prepared by cross-linking Gln-41 and Cys-374 residues of two adjacent actin protomers with a photo-activated heterobifunctional reagent *N*-(4-azido-2-nitrophenyl) putrescine (ANP), as described earlier (21, 31). To decrease the amount of higher-order actin oligomers, cross-linking was carried out with copolymers made from equal amounts of ANP-labeled (by means of transglutaminase reaction) and unlabeled actin. After UV irradiation, 1.0 mM DTT was added to quench the unreacted arylazido compound, and the cross-linked filaments were extensively dialyzed with three changes of DTT-free G-buffer (pH 7.5). After that the unmodified Cys-374 on actin protomers was labeled with 2-fold molar excess of tetramethyl rhodamine maleimide. The mixture of cross-linked oligomers and monomers was concentrated and fractionated on Sephacryl S200 (Amersham Pharmacia Biosciences) gel-filtration 90/2.5-cm column. Fractions enriched with longitudinal dimers were combined, concentrated, and fractionated as described in *Supporting Materials and Methods*.

Crystallization and Data Collection. The skeletal actin dimer was crystallized by using the hanging drop method, with the drop consisting of 2.5 μl of the final actin dimer mixture (3 mg/ml actin plus a 1.25:1 molar ratio of latrunculin A to actin monomer), 2 μl of the reservoir solution (500 μl of 35% 2-methyl-2,4-pentanediol/100 mM sodium acetate, pH 4.7/20 mM calcium chloride), and 0.5 μl of 3 M nondetergent sulfobetaine 195 (Hampton Research, Aliso Viejo, CA) as the additive. The crystals belonged to space group C2 containing one actin monomer in the asymmetric unit. An x-ray diffraction data set was collected on a native crystal at the Advanced Light Source beamline 8.2.2 equipped with a Quantum 315 charge-coupled device detector (Area Detector Systems Corporation, Poway, CA). Data extending to 2.5 Å were collected at a wavelength of 1.1 Å at 100 K without the need for additional cryoprotectant.

Structure Solution and Refinement. The crystal structure was determined by molecular replacement using the program EPMR (32), with rabbit actin monomer (Protein Data Bank ID code 1QZ5) serving as the search model, and subsequently refined (*Supporting Materials and Methods*). The geometric quality of the model was assessed with the structure validation tools PROCHECK (33) and WHATIF (34). Protein structures were illustrated by using the program PYMOL (35). Coordinates for the actin dimer have been deposited in the Protein Data Bank (PDB ID code 2A5X).

Construction of an F-Actin Filament Model from the Dimer Crystal Structure. An optimal model for the F-actin filament was constructed by performing a fine search over the rigid body parameters describing the orientation and position of the actin protomer relative to the fixed coordinate system of the F-actin helix. (Further details are provided in *Supporting Materials and Methods*). The target function minimized was a sum of two terms, one describing the deviation from the Holmes filament model (15) and the other describing deviations at the dimer interface in the candidate filament model compared with the crystal structure reported here. Filaments constructed according to these criteria showed very good agreement with experimental density maps generated from EM and diffraction studies (see Fig. 4). In this crystal-based filament model, the protomer is rotated 15° relative to that in the Holmes model. This rotation corresponds to a rms coordinate deviation of 4.3 Å between the atoms in the crystal-based F-actin model and those in the Holmes model. The rms coordinate deviations at the dimer interface are 2.8 Å when compared with the dimer crystal structure. Coordinates for the filament model are available from the authors upon request.

Results and Analysis

Because assembled actin filaments cannot be crystallized, the goal of understanding their high-resolution structure may be best approached by crystallizing defined actin oligomers that would mimic the arrangement of protomers in F-actin. The longitudinal (or vertical) contact between two actin protomers in one strand serves as a logical starting point for defining the critical interfaces between molecules. Longitudinal dimers are of particular interest for structure determination because many actin-binding proteins attach to two longitudinally adjacent protomers in F-actin. Some information is already available regarding the approximate regions of contact between molecules at this interface (18–21). A more detailed view of the interface would effectively define the strand structure in F-actin and also could constrain models of the complete double-stranded filament.

The best strategy for isolating defined actin oligomers has been to stabilize interprotomer contacts in the filament state by specific, covalent cross-linking and then to depolymerize and purify the cross-linked oligomers. Previously, we reported that an actin longitudinal dimer can be stabilized by cross-linking the Gln-41 and Cys-374 residues of two adjacent actin protomers with a heterobifunctional photo-activated reagent, ANP (21, 31, 36). The purified ANP cross-linked dimers can be readily reassembled into filaments (in the presence of Mg^{2+}). Extensive characterization of the ANP cross-linked filaments revealed little, if any, effect of the cross-linking on kinetic and equilibrium parameters for the S1 myosin interaction with actin, including the K_m and V_{max} values of the actomyosin ATPase (20). These results indicate that ANP cross-linking preserves actin function. The inhibited *in vitro* sliding observed in these filaments is most likely due to impediments to the structural transitions that are needed for force generation (20). Indeed, EM reconstruction of similarly cross-linked actin filaments (by a disulfide bond between Cys-41 and Cys-374 in a yeast actin mutant) revealed only minor structural perturbations (14). ANP cross-linking was therefore an attractive approach to the crystallization of native-like longitudinal actin dimers.

A multistep protocol was used to prepare and purify stable actin longitudinal dimers, as described in Fig. 1 (also see *Materials and Methods*). To prevent the subsequent polymerization of these actin dimers under crystallization conditions, we

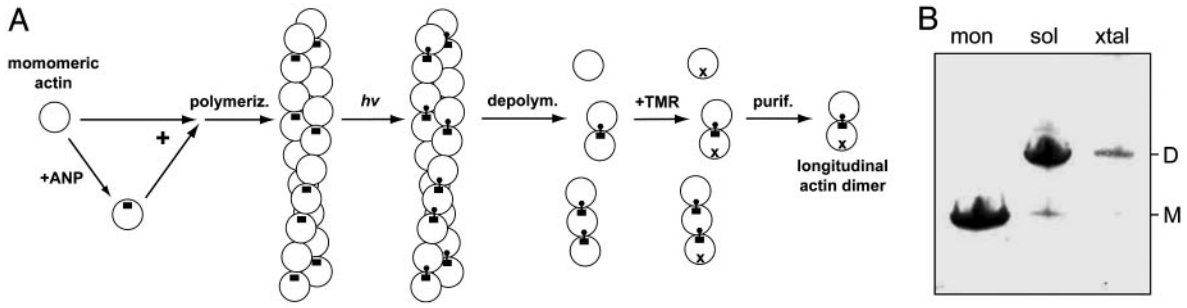

Fig. 1. Preparation of cross-linked actin dimer. (*A*) An illustration of the strategy used to isolate an actin dimer, cross-linked along the longitudinal direction of the filament (see *Materials and Methods*). F-actin filaments were polymerized from a mixture of unlabeled G-actin and actin labeled with the photoactivatable cross-linking reagent, ANP (black rectangles). After light-induced cross-linking (from Gln-41 to Cys-374 on the protomer above), actin was depolymerized and blocked from further polymerization by tetramethylrhodamine (black X). (*B*) SDS/PAGE confirming that the crystals and the protein sample from which they grow are both predominantly dimeric. Monomeric and dimeric molecular weights are indicated by M and D, respectively. The crystal sample is indicated by xtal, the purified dimer in solution is indicated by sol, and, as a control, monomeric G-actin is indicated by mon.

used a combination of two strategies. The modification of Cys-374 at the dimer's barbed end with tetramethyl rhodamine maleimide, which prevents the polymerization of G-actin (4, 37), did not fully block the polymerization of cross-linked dimers. Therefore, the actin depolymerizing drug latrunculin A was added to these preparations to further inhibit the polymerization of ANP cross-linked dimers (see *Supporting Materials and Methods*). Crystals diffracting to a resolution of 2.5 Å were obtained when latrunculin A was bound to the protein, and when the nonhydrolizable ATP analog, adenosine 5′-[β,γ-imido]triphosphate, was also bound in the nucleotide pocket. The crystal space group was C2 with unit cell dimensions $a = 207.4$ Å, $b = 54.4$ Å, $c = 36.2$ Å, and $\beta = 98.6°$.

The crystal structure of the actin dimer was determined by the molecular replacement method. The crystal contains only one actin protomer in the asymmetric unit, making it impossible to visualize the cross-link between protomers, which must be present at only half of the equivalent positions in the crystal. Residues 38–65, representing much of subdomain 2, also were found to be disordered in the crystal, as discussed subsequently. Aside from this part of subdomain 2 and the terminal residues (1–4 and 375), the remainder of the protein structure (residues 5–37 and 66–374) was successfully built and refined, including the adenosine 5′-[β,γ-imido]triphosphate and latrunculin A ligands, as described in *Materials and Methods* and Table 2, which is published as supporting information on the PNAS web site.

The crystal structure of the actin dimer revealed protomers arranged head to tail along the **b**-axis of the crystal. The similarity between the organization of actin protomers in the crystal and the organization proposed in current models of F-actin is immediately apparent (Fig. 2). The unit cell spacing between protomers in the crystal very nearly matches the known axial rise in the F-actin filament. The crystal **b**-axis is 54.4 Å, whereas the F-actin axial rise along a protofilament strand takes a value of 55 Å (with some variation between experiments) (Fig. 2). The protomer arrangements are so similar overall that two adjacent protomers taken from each of the two structures [i.e., the dimer crystal and an F-actin model (11)] can be superim-

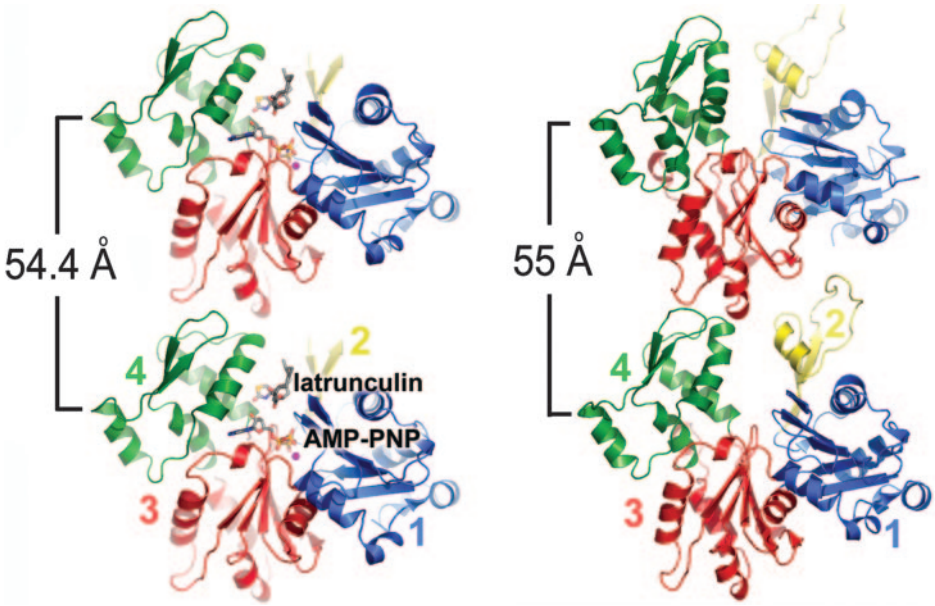

Fig. 2. Crystal structure of the longitudinal actin dimer and its overall similarity to a current model of F-actin. In the actin dimer crystal (*Left*), unit cell translations along the **b**-axis of the crystal (vertical) generate a filament whose protomer orientations and longitudinal contacts resemble those seen in Holmes' actin fibril model (*Right*) (11). Actin subdomains 1, 2, 3, and 4 are colored blue, yellow, red, and green, respectively. In the actin dimer, parts of subdomain 2 and its cross-link to the protomer above are not visualized because of disorder in the crystal.

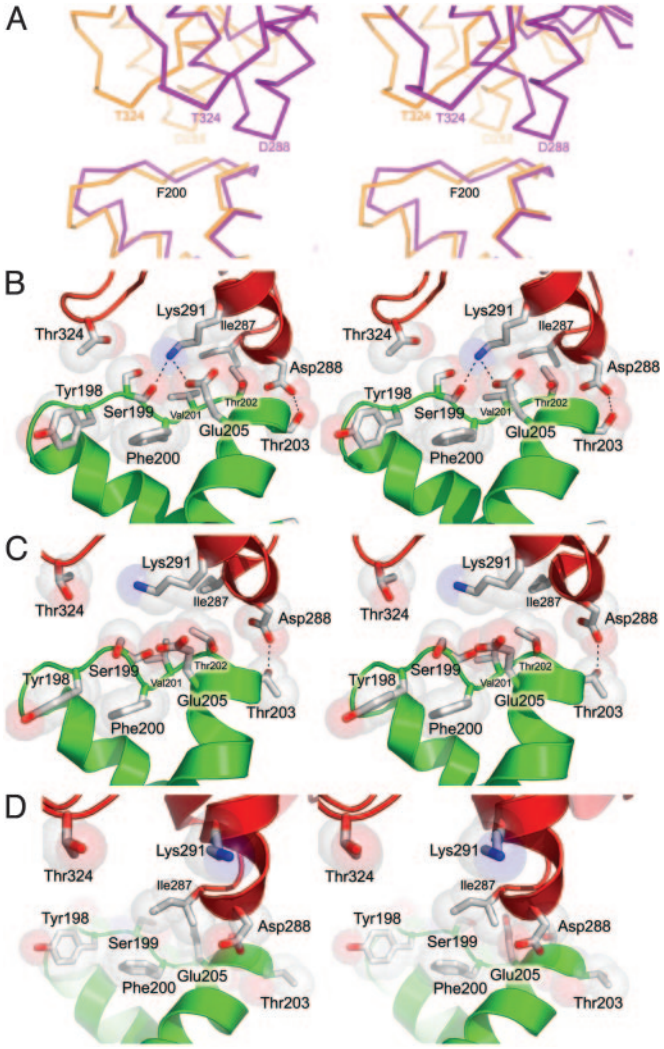

Fig. 3. Models of the longitudinal contact between actin molecules shown in stereoview, focusing on the interface between the top and bottom protomers. (*A*) A comparison of the actin dimer crystal structure (yellow) with two protomers from a current model of the F-actin filament (magenta) (15). (*B*) A detailed view of the longitudinal actin interface observed in the actin dimer. (*C*) A detailed view of a similar interface observed in a crystal contact of an actin–FH2 complex (29). (*D*) A detailed view of the corresponding interface from a current F-actin filament model (15) showing significant differences at the side-chain level compared with *B* and *C*.

posed with a rms coordinate deviation of only 5.0 Å over all α-carbon backbone atoms. This agreement is particularly striking in view of the absence from the crystal dimer of the slow twist known to exist between protomers along one strand of F-actin. In F-actin, two such protomers are related by an $\approx$28° rotation, whereas the corresponding protomers in the crystal dimer are related by pure translation.

The major interactions in the actin dimer crystal occur between subdomain 4 of the lower protomer and subdomain 3 of the upper protomer (Fig. 3 *A* and *B*). We see close interactions between residues 197–204 in subdomain 4 (residue numbers correspond to rabbit α-skeletal actin sequence) of the lower protomer, with residues 287–291 and 322–326 in subdomain 3 of the upper protomer. In particular, we see the Lys-291 side chain forming both a salt bridge with Glu-205 and a hydrogen bond with the backbone carbonyl of Ser-199. An additional hydrogen bond is formed between the Asp-288 and Thr-203 side chains.

Table 1. Contacts between neighboring protomers in the actin dimer crystal and corresponding longitudinal contacts in a current F-actin model

			Distance, Å	
Protomer 1	Protomer 3	Interaction type*	Dimer crystal	F-actin model†
E205 (OE2)	K291 (NZ)	SB	2.8	20.0
S199 (O)	K291 (NZ)	HB	2.9	25.1
T203 (OG1)	D288 (OD2)	HB	2.9	9.8
G197 (O)	T324 (CG2)	VDW	3.3	20.9
S199 (CB)	T324 (OG1)	VDW	3.3	21.5
T202 (CG2)	I287 (O)	VDW	3.5	11.0
D244 (CB)	K326 (NZ)	VDW	3.4	16.9

*SB, salt bridge; HB, hydrogen bond; VDW, van der Waals contact.
†Ref. 15.

Intermolecular interactions visualized are shown in Fig. 3*B* and summarized in Table 1.

Several lines of evidence support the contention that the atomic interactions visualized in the crystal dimer represent interactions present in F-actin filaments. In sequence alignments of actin from multiple species, these interface residues are highly conserved (38). In a few organisms, one or both amino acid residues of the Glu-205–Lys-291 pair are conservatively substituted with residues capable of forming hydrogen bonds. In one case, that of *Paramecium tetraurelia*, in which residue Glu-205 is substituted with glutamine, this change is accompanied by the mutation of Lys-291 to Glu (GenBank database). The second amino acid residue pair connected by a hydrogen bond, Asp-288 and Thr-203, was tested by preparing two separate mutants of yeast actin, one bearing Cys in place of Asp-288 and the other bearing Cys in place of Thr-203 (as well as a C374S mutation). After the two mutant forms of actin were copolymerized, they could be readily cross-linked with a short bifunctional reagent, 1,1-methanediyl bismethanethiosulfonate (MTS-1-MTS). Cross-linking did not occur in filaments of the T203C/C374S mutant, in filaments of wild-type actin alone (data not shown), or in the copolymer with wild-type actin (see Fig. 5, which is published as supporting information on the PNAS web site). This result supports the argument for close proximity of the mutated Cys-203 and Cys-288 residues in the native actin filament.

Further evidence for the relevance of the molecular interface visualized in the cross-linked dimer comes from a recent crystal structure of a formin homology (FH2) domain in complex with actin (29). The FH2 domain binds two actin protomers related laterally (i.e., across two adjacent strands). However, in this crystal as well there is an additional contact between actin protomers related by a pure translation of 56.2 Å. This spacing is similar to the actin strand axial rise, and the interface (Fig. 3C) is strikingly similar to the one observed in our cross-linked dimer (Fig. 3*B*). In particular, the hydrogen bond we see between Asp-288 and Thr-203 also is seen in the crystal contact in the actin–FH2 complex structure. Residues Lys-291 and Glu-205 are also in proximity as we observe, although the specific hydrogen bond is not formed between actin protomers in the actin–FH2 complex. The reappearance of this highly similar interface in two entirely unrelated crystal forms of actin provides strong support for the conclusion that the interface is one that would be energetically favorable in the native filament and is not a fortuitous consequence of crystallization.

The amino acids we see making specific interactions in the actin dimer crystal are in somewhat different locations compared with currently accepted models of F-actin (Fig. 3 *A* and *D*). For example, α-carbon atoms of residues Lys-291 and Glu-205 from adjacent protomers are 9 Å apart in the crystal but 16 Å

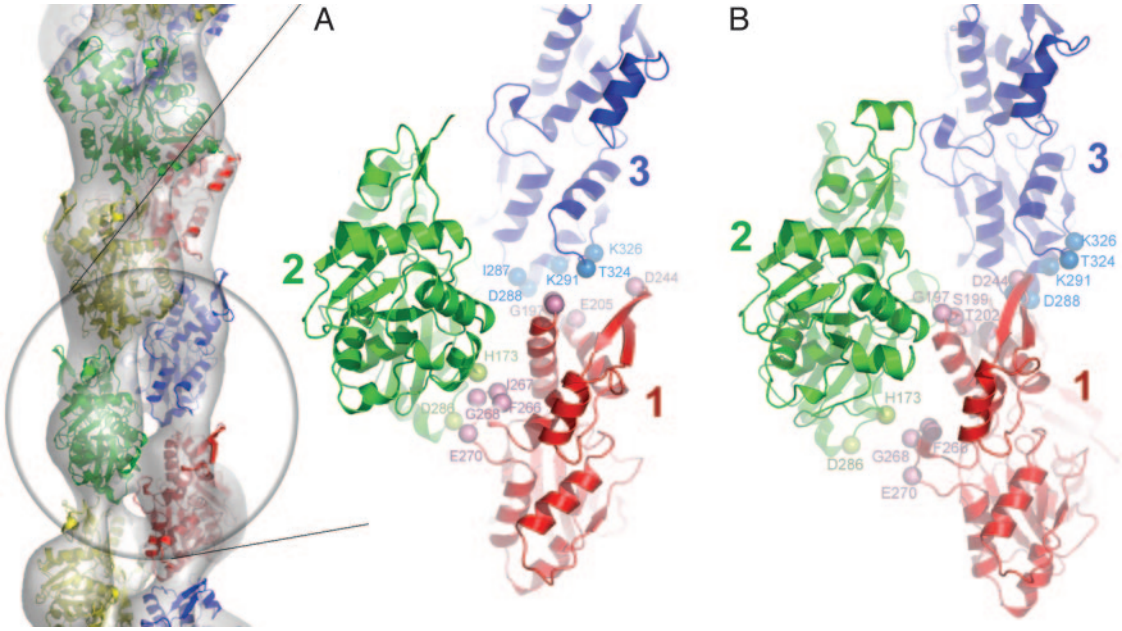

Fig. 4. Models of F-actin structure. (*A*) Fit of a plausible crystal-based F-actin model (see text) to an EM reconstruction taken from Orlova *et al.* in 2001 (14) and a close-up view of three subunits from such a model. Residues lining the protomer interfaces are labeled and protomers are numbered to match those listed in Tables 1 and 3. Protomers are colored individually. Subdomain 2 is shown in the conformation it adopts in other actin structures, leaving out the variable DNaseI binding loop. (*B*) The Holmes *et al.* (15) F-actin model from 2003 viewed in the same orientation. Labeled residues correspond to those in *A*.

apart in the recently revised Holmes model of F-actin (15). When comparing the entire interfacial region of the crystal dimer with the same region in a model of F-actin (11), the rms coordinate differences are 6.3 Å over backbone atoms. A few considerably larger differences are seen when comparing amino acid side chains, because some side chain conformations differ between the models. Furthermore, when examining distances between pairs of atoms in the interface (Table 1), the discrepancies between models tend to be amplified by coordinate shifts of interacting protomers in opposite directions. Nonetheless, the discrepancies observed here between the actin dimer crystal and current models of F-actin are within the bounds of uncertainty in models of F-actin, which are based on fiber diffraction and imaging data in the 8- to 10-Å resolution range. Hence, it can be argued that the particular interface between subdomains 3 and 4 visualized in the present work is consistent with previous structural data on F-actin filaments.

Discussion

With regard to the goal of constructing an atomic resolution model of F-actin, our crystal structure of an actin dimer suffers from two principle shortcomings: the disordered subdomain 2 and the untwisting or straightening of the protofilament strand. As a result of the disorder in subdomain 2, contacts that are likely to be present in the native filament (between subdomain 2 from the lower protomer and subdomain 1 from the upper protomer) are not visualized in the crystal. Mobility and conformational variability in subdomain 2, although less extensive than seen here, has been reported in various models and biophysical studies (39–42). Furthermore, the tendency of subdomain 2 to show disorder is likely exacerbated by that region existing in two chemically distinct states (i.e., cross-linked and non-cross-linked) in the crystal form obtained here, with the crystal providing only an averaged view of the two conformations expected (see *Supporting Materials and Methods*). Regardless of the reason for the disorder in subdomain 2, the picture that emerges from the structure of the actin dimer is that one major interprotomer contact in the F-actin filament (between subdomains 3 and 4) appears to be preserved, whereas a more dynamic contact (between subdomains 2 and 1), which could be present in native filaments when there is a slight rotation between protomers, is killed to form an ordered crystal lattice.

The second deficiency, the presence in the crystal of a single straight protofilament strand, presents two problems. By itself, the structure of a single straight strand provides no direct information about lateral interactions between protomers on opposite strands. Furthermore, the straight strand observed in the crystal does not provide sufficient geometric constraints for construction of the desired two-stranded model. In particular, in attempting to introduce a second strand, and the known helical twist, it is not clear precisely where the helical axis of the native filament should be positioned or oriented relative to the straight strand observed. Nonetheless, the importance of attempting a reconstruction of a native-like (two-stranded) filament is clear. Besides producing potentially plausible models for further examination, such an exercise makes it possible to ask whether the molecular interface that has been visualized in this study is, in fact, consistent with a native-like filament. Therefore, to overcome the problems noted above, additional structural constraints were adopted.

We combined the present crystal structure information on the longitudinal interface with earlier results from fiber diffraction and EM to produce a revised model of the F-actin filament that is consistent as nearly as is possible with both types of data. To accomplish this goal, a computer program was written to determine the orientation and position of actin protomers in a filament that would deviate the least from the combined constraints. The helical parameters for F-actin were taken as known quantities, as was the approximate position of the protomers from the helical axis. It was possible to obtain a family of closely related structural models for the F-actin filament in which the crystallographically observed longitudinal interface was preserved (with differences in atomic positions in the range of 2–4 Å), whereas the orientation of the actin protomer deviated from those in various other models for F-actin by ≈15° (Fig. 4). A 15° rotation of the actin protomer results in average atomic dis-

placements of only 4.3 Å over the protein backbone atoms. Taking the resolution of previous studies into account, together with the observation of comparable deviations of protomer rotation and filament twist in multiple EM studies (25, 43), we consider these differences to be within the bounds of molecular flexibility and uncertainty in various models.

The F-actin filament model arising from this exercise (Fig. 4) is no longer derived strictly from experiment and may represent only one of multiple equally good models. Nonetheless, it serves to demonstrate that a plausible model for the F-actin filament can be constructed while nearly preserving the molecular interface visualized here by crystallography. Furthermore, it seems noteworthy that the resulting model does not lead to severe collisions between the first and second strands. On the contrary, the construction results in a somewhat more intimate interaction between strands than what was reported in the original Holmes model of F-actin, where swinging and insertion of a hydrophobic loop (residues 262–274) into the opposite strand had to be invoked to hold together the separate strands (11). The F-actin model produced here is also consistent with density maps generated for F-actin from a variety of experimental methods. The agreement with the map of Orlova *et al.* (14) is shown in Fig. 4. The fit of our model to this map is nearly equal to the fit of the Holmes *et al.* (15) model to the same map, with correlation coefficients of 0.73 and 0.77, respectively. The near equivalence in correlation of the two models is notable, considering that our model, unlike the Holmes *et al.* (15) model, introduces no rotations between subdomains and also satisfies our crystal contact constraints. Keeping in mind the tentative nature of our model for the complete F-actin filament, we note potential interactions between residues Phe-266 and Glu-270 on one protomer (the same hydrophobic loop as mentioned above) and between His-173 and Asp-286 on the laterally related protomer (Fig. 4). These residues are closer together in our model of F-actin compared with earlier models. Furthermore, their proximity agrees with the lateral interactions in the FH2 complex consisting of residues Gly-268–Glu-270 from protomer 1 and Met-283-Asp–288 from protomer 2 (see Table 3, which is published as supporting information on the PNAS web site) (29).

Concluding Remarks

The crystal structure of the longitudinal actin dimer provides an atomic resolution view of a molecular interface between actin protomers, generally consistent with previous studies on native F-actin filaments. At least for one of the contact regions (from subdomain 3 to 4) between longitudinally related protomers, there is now good evidence for which amino acid residues are involved in specific molecular interactions in the filament. The dimer crystal structure confirms the basic features of previous filament models, while it modifies these earlier views in significant ways. By using the interactions visualized in the crystal as a constraint, a speculative step can be taken to construct a plausible model for F-actin. Although this model could be useful for generating hypotheses for testing, structures of additional actin subassemblies will be required to define the complete structure of F-actin and its complexes with other proteins at atomic resolution.

We thank D. Cascio and J. Beck for technical assistance; E. Egelman and S. Almo for helpful comments on the manuscript; the staff at Advanced Light Source beamline 8.2.2 for technical support; E. Egelman, D. Hanein, R. Milligan, and W. Lehman for providing us with density maps of F-actin; K. Holmes for supplying coordinates of F-actin models; and P. Rubenstein and M. McKane (Iowa University) for help with preparation of yeast actin mutants. This work was supported by National Institutes of Health Grants GM31299 (to T.O.Y.) and AR20231, National Science Foundation Grant MCB0316269 and an American Heart Association Greater Los Angeles Affiliates grant (to E.R.), and Országos Tudományos Kutatási Alapprogramok Grant T-034874 (to G.H.).

1. Kreis, T. & Vale, R. (1999) *Guidebook to the Cytoskeletal and Motor Proteins* (Oxford Univ. Press, Oxford).
2. Kabsch, W., Mannherz, H. G., Suck, D., Pai, E. F. & Holmes, K. C. (1990) *Nature* **347,** 37–44.
3. Vorobiev, S., Strokopytov, B., Drubin, D. G., Frieden, C., Ono, S., Condeelis, J., Rubenstein, P. A. & Almo, S. C. (2003) *Proc. Natl. Acad. Sci. USA* **100,** 5760–5765.
4. Otterbein, L. R., Graceffa, P. & Dominguez, R. (2001) *Science* **293,** 708–711.
5. Graceffa, P. & Dominguez, R. (2003) *J. Biol. Chem.* **278,** 34172–34180.
6. McLaughlin, P. J., Gooch, J. T., Mannherz, H. G. & Weeds, A. G. (1993) *Nature* **364,** 685–692.
7. Chik, J. K., Lindberg, U. & Schutt, C. E. (1996) *J. Mol. Biol.* **263,** 607–623.
8. Morton, W. M., Ayscough, K. R. & McLaughlin, P. J. (2000) *Nat. Cell Biol.* **2,** 376–378.
9. Klenchin, V. A., Allingham, J. S., King, R., Tanaka, J., Marriott, G. & Rayment, I. (2003) *Nat. Struct. Biol.* **10,** 1058–1063.
10. Sablin, E. P., Dawson, J. F., VanLoock, M. S., Spudich, J. A., Egelman, E. H. & Fletterick, R. J. (2002) *Proc. Natl. Acad. Sci. USA* **17,** 10945–10947.
11. Holmes, K. C., Popp, D., Gebhard, W. & Kabsch,W. (1990) *Nature* **347,** 44–49.
12. Hanein, D., Volkmann, N., Goldsmith, S., Michon, A. M., Lehman, W., Craig, R., DeRosier, D., Almo, S. & Matsudaira, P. (1998) *Nat. Struct. Biol.* **5,** 787–792.
13. Milligan, R. A., Whittaker, M. & Safer, D. (1990) *Nature* **348,** 217–221.
14. Orlova, A., Galkin, V. E., VanLoock, M. S., Kim, E., Shvetsov, A., Reisler, E. & Egelman, E. H. (2001) *J. Mol. Biol.* **312,** 95–106.
15. Holmes, K. C., Angert, I., Kull, F. J., Jahn, W. & Schroder, R. R. (2003) *Nature* **425,** 423–427.
16. Hodgkinson, J. L., el-Mezgueldi, M., Craig, R., Vibert, P., Marston, S. B. & Lehman, W. (1997) *J. Mol. Biol.* **273,** 150–159.
17. Aebi, U., Millonig, R., Salvo, H. & Engel, A. (1986) *Ann. N.Y. Acad. Sci.* **483,** 100–119.
18. Elzinga, M. & Phelan, J. J. (1984) *Proc. Natl. Acad. Sci. USA* **81,** 6599–6602.
19. Kim, E., Wriggers, W., Phillips, M., Kokabi, K., Rubenstein, P. A. & Reisler, E. (2000) *J. Mol. Biol.* **299,** 421–429.
20. Kim, E., Bobkova, E., Hegyi, G., Muhlrad, A. & Reisler, E. (2002) *Biochemistry* **41,** 86–93.
21. Hegyi, G., Mak, M., Kim, E., Elzinga, M., Muhlrad, A. & Reisler, E. (1998) *Biochemistry* **37,** 17784–17792.
22. Guan, J. Q., Takamoto, K., Almo, S. C., Reisler, E. & Chance, M. R. (2005) *Biochemistry* **44,** 3166–3175.
23. van den Ent, F., Amos, L. A. & Lowe, J. (2001) *Nature* **413,** 39–44.
24. van den Ent, F., Moller-Jensen, J., Amos, L. A., Gerdes, K. & Lowe, J. (2002) *EMBO J.* **21,** 6935–6943.
25. Schmid, M. F., Sherman, M. B., Matsudaira, P. & Chiu, W. (2004) *Nature* **431,** 104–107.
26. Dawson, J. F, Sablin, E. P., Spudich, J. A. & Fletterick, R. J. (2003) *J. Biol. Chem.* **278,** 1229–1238.
27. Klenchin, V. A., King, R., Tanaka, J., Marriott, G. & Rayment, I. (2005) *Chem. Biol.* **12,** 287–291.
28. Bubb, M. R., Govindasamy, L., Yarmola, E. G., Vorobiev, S. M., Almo, S. C., Somasundaram, T., Chapman, M. S., Agbandje-McKenna, M. & McKenna, R. (2002) *J. Biol. Chem.* **277,** 20999–21006.
29. Otomo, T., Tomchick, D. R., Otomo, C., Panchal, S. C., Machius, M. & Rosen, M. K. (2005) *Nature* **433,** 488–494.
30. Spudich, J. A. & Watt, S. (1971) *J. Biol. Chem.* **246,** 4866–4871.
31. Kim, E., Bobkova, E., Miller, C. J., Orlova, A., Hegyi, G., Egelman, E. H., Muhlrad, A. & Reisler, E. (1998) *Biochemistry* **37,** 17801–17809.
32. Kissinger, C. R., Gehlhaar, D. K. & Fogel, D. B. (1999) *Acta Crystallogr. D* **55,** 484–489.
33. Laskowski, R. A., MacArthur, M. W., Moss, D. S. & Thornton, J. M. (1993) *J. Appl. Crystallogr.* **26,** 283–291.
34. Vriend, G. & Sander, C. (1993) *J. Appl. Crystallogr.* **26,** 47–60.
35. DeLano, W.L. (2002) *The* PYMOL *User's Manual* (DeLano Scientific, San Carlos, CA).
36. Kim, E., Phillips, M., Hegyi, G., Muhlrad, A. & Reisler, E. (1998b) *Biochemistry* **37,** 17793–17800.
37. Kudryashov, D. S., Phillips, M. & Reisler, E. (2004) *Biophys. J.* **87,** 1136–1145.
38. Altschul, S. F., Madden, T. L., Schäffer, A. A., Zhang, J., Zhang, Z., Miller, W. & Lipman, D. J. (1997) *Nucleic Acids Res.* **25,** 3389–3402.
39. Orlova, A. & Egelman, E. H. (1992) *J. Mol. Biol.* **227,** 1043–1053.
40. Orlova, A. & Egelman, E. H. (1993) *J. Mol. Biol.* **232,** 334–341.
41. Muhlrad, A., Cheung, P., Phan, B. C., Miller, C. & Reisler, E. (1994) *J. Biol. Chem.* **269,** 11852–11858.
42. Khaitlina, S. Y. & Strzelecka-Golaszewska, H. (2002) *Biophys J.* **82,** 321–334.
43. Galkin, V. E., VanLoock, M. S., Orlova, A. & Egelman, E. H. (2002) *Curr. Biol.* **12,** 570–575.